Prostate imaging features that indicate benign or malignant pathology on biopsy

Catherine Elizabeth Lovegrove[1,2], Mudit Matanhelia[1,2], Jagpal Randeva[1,2], David Eldred-Evans[1,2], Henry Tam[1,2], Saiful Miah[1,2], Mathias Winkler[1,2], Hashim U. Ahmed[1,2], Taimur T. Shah[1,2]

[1]Division of Surgery, Department of Surgery and Cancer, Imperial College London, London, UK; [2]Imperial Urology, Charing Cross Hospital, Imperial College Healthcare NHS Trust, London, UK

Contributions: (I) Conception and design: None; (II) Administrative support: None; (III) Provision of study materials or patients: None; (IV) Collection and assembly of data: None; (V) Data analysis and interpretation: None; (VI) Manuscript writing: All authors; (VII) Final approval of manuscript: All authors.

Correspondence to: Catherine Elizabeth Lovegrove. Division of Surgery, Department of Surgery and Cancer, Imperial College London, London, UK. Email: catherinelovegrove1@gmail.com.

Abstract: Accurate diagnosis of clinically significant prostate cancer is essential in identifying patients who should be offered treatment with curative intent. Modifications to the Gleason grading system in recent years show that accurate grading and reporting at needle biopsy can improve identification of clinically significant prostate cancers. Extracapsular extension of prostate cancer has been demonstrated to be an adverse prognostic factor with greater risk of metastatic spread than organ-confined disease. Tumor volume may be an independent prognostic factor and should be considered in conjunction with other factors. Multiparametric magnetic resonance imaging (MP-MRI) has become an increasingly important tool in the diagnosis and characterization of prostate cancer. MP-MRI allows T2-weighted (T2W) anatomical imaging to be combined with functional and physiological assessment. Diffusion-weighted imaging (DWI) has shown greater sensitivity, specificity and negative predictive value compared to prostate specific antigen (PSA) testing and T2W imaging alone and has a more positive correlation with Gleason score and tumour volume. Dynamic gadolinium contrast-enhanced (DCE) imaging can exhibit difficulties in distinguishing prostatitis from malignancy in the peripheral zone, and between benign prostatic hyperplasia (BPH) and malignancies in the transition zone (TZ). Computer aided diagnosis utilizes software to aid radiologists in detecting and diagnosing abnormalities from diagnostic imaging. New techniques of quantitative MRI, such as VERDICT MRI use tissue-specific factors to delineate different cellular and microstructural phenotypes, characterizing tissue properties with greater detail. Proton MR spectroscopic imaging (MRSI) is a more technically challenging imaging modality than DCE and DWI MRI. Over the last decade, choline and prostate-specific membrane antigen (PSMA) positron emission tomography (PET) have developed as better tools for staging than conventional imaging. While hyperpolarized MRI shows promise in improving the imaging and differentiation of benign and malignant lesions there is further work required. Accurate reading and interpretation of diagnostic investigations is key to accurate identification of abnormal areas requiring biopsy, sparing those in whom benign or indolent disease can be managed by non-invasive means. Embracing and advancing existing technologies is essential in furthering this process.

Keywords: Prostate; magnetic resonance imaging (MRI); imaging; quantitative; qualitative; benign; malignant; parametric

Introduction

Accurate diagnosis of clinically significant prostate cancer is essential in identifying patients who should be offered treatment with curative intent. Traditionally, the diagnosis of prostate cancer has been made solely by transrectal ultrasound (TRUS) guided biopsy. This can result in the over-diagnosis and subsequent overtreatment of low-grade prostate cancer, but may also fail to detect clinically significant cancers. Multi-parametric magnetic resonance imaging (MP-MRI) has become an increasingly important tool in the diagnosis and characterization of prostate cancer (1). Traditional prostate MRI consisted of only T1-weighted (T1W) and T2-weighted (T2W) imaging, and could only be used for local staging in known prostate cancer. MP-MRI allows T2W anatomical imaging to be combined with functional and physiological assessment. Sequences using diffusion-weighted imaging (DWI) and dynamic gadolinium contrast-enhanced (DCE) imaging can greatly aid in the detection of clinically significant cancer. Accurate reading and interpretation of MP-MRI imaging is key to the accurate identification of abnormal areas which require biopsy, and those which represent benign or indolent disease which might avoid a biopsy. Herein, we review the literature on qualitative and quantitative MRI parameters which can distinguish between malignant and benign disease.

Determining clinically significant prostate cancer

Clinically significant prostate cancer is frequently categorized according to three main prognostic factors as defined by Stamey and Epstein (2,3):

(I)   Gleason score 7 or greater (3+4=7 or higher);
(II) Extraprostatic tumor extension (T3a disease or greater);
(III) Tumor volume on whole-mount prostatectomy >0.5 cm^3 (although on biopsy different groups use different criteria such as number of biopsies positive or percentage cancer involvement or millimetres of cancer per core).

This definition is derived from the seminal work of Hanahan and Weinberg (4). These lesions exhibit more malignant behaviour and are more likely to warrant treatment compared to smaller, less aggressive tumours that can be inconsequential (5). The parameters used to define clinically significant prostate cancer aid in prognostication

of prostate cancer. However, these parameters are not used in isolation for clinical decision making where further patient characteristics including comorbidities, age, performance status and patient choice will further contribute.

Gleason score

The Gleason score for prostate cancer was developed in the 1960s (6). This scoring system analyzed glandular patterns within prostate biopsy samples and assigned 2 grades to any malignancy detected, based upon the predominant pattern and second-most common pattern. Total scores ranged from 2–10, and an increased score was associated with increased cancer-specific mortality.

The Gleason grading system was initially revised at the 2005 International Society of Urological Pathology (ISUP) Consensus Conference (7). Importantly, this recommended that Gleason grades 2–5 would only be given in rare circumstances, effectively making Gleason 6 the lowest pathological risk category. Furthermore, it further defined the criteria for Gleason pattern 3 and pattern 4. Cribriform growth patterns that were included in the original pattern 3 were largely removed and placed into pattern 4. The further ISUP Consensus update in 2014 placed all cribriform patterns into Gleason pattern 4. Glomeruloid glands are now also graded as pattern 4, as well as ill-defined glands with poorly formed glandular lumina (8).

The main impact of the modified Gleason grading was an increase in the reporting of higher Gleason scores (9). Studies report improved correlation between needle biopsy and Gleason grade, stage at final radical prostatectomy specimen and subsequent biochemical recurrence on follow-up since the modified system was adopted (10,11). Furthermore, reassignment of the classical cribriform pattern 3 to pattern 4 has been shown to be valuable in predicting biochemical recurrence following radical prostatectomy (12).

In addition to the Gleason score attributed to biopsy samples, reporting of percentage of Gleason pattern 4 within biopsy samples found to be Gleason 7 has demonstrated improved stratification regarding risk of disease progression. This sub-classification enables identification of men with relatively insignificant prostate cancer (13). Tertiary high-grade Gleason patterns correlate with more aggressive disease and worse prognosis secondary to different pathologic stage and biochemical progression.

The modifications to the Gleason grading in recent years

Table 1 Grouped grading system for prostate cancer derived from Epstein *et al.* [2016]

Grading group	Gleason score	Histological appearances
1	3+3=6	Individual discrete well-formed glands only
2	3+4=7	Predominantly well-formed glands, lesser component of poorly formed/fused/cribriform glands
3	4+3=7	Predominantly poorly formed/fused/cribriform glands, lesser component of well-formed glands
4	8	Poorly formed/fused/cribriform glands or predominantly well-formed glands, lesser component lacking glands or predominantly lacking glands, lesser component of well-formed glands
5	9–10	Lack of gland formation (or with necrosis) +/− poorly formed/fused/cribriform glands

shows that accurate grading and reporting at needle biopsy can help to identify clinically significant prostate cancers. Where the D'Amico classification failed to differentiate between Gleason score 3+4=7 and 4+3=7 there has been increasing recognition that the latter demonstrates a significantly worse prognosis with greater likelihood of progression following therapy (14). Grouping of Gleason scores by Pierorazio *et al.* formulated five grades of prostate cancer to stratify patients further according to prognosis and identify those with a greater likelihood of requiring treatment (10). Epstein *et al.* subsequently demonstrated the five-group grading system with histological parameters to result in more accurate risk stratification of lesions with the additional benefit of being simpler, especially from the patient's perspective (15). A significant, inverse correlation is demonstrated between increasing group grading and recurrence-free progression following radical prostatectomy or radiotherapy, formulating the grading groups as in *Table 1*.

Extraprostatic tumor extension

Extracapsular extension of prostate cancer has been demonstrated to be an adverse prognostic factor with greater risk of metastatic spread than organ-confined disease. Wheeler *et al.* stated that the likelihood of metastatic progression was directly linked to invasion into or through the prostatic capsule, with worse progression-free probabilities in patients whose tumors breached the prostatic capsule (16). Furthermore, pT3 disease carries a greater risk of positive margins at radical prostatectomy with Hull *et al.* finding significantly different progression-free probability at 10 years following radical retropubic prostatectomy when comparing tumors confined versus those not confined to the prostate (17). These factors contribute to reduced likelihood of establishing long-term cancer control in patients.

Tumor volume

Another important concept in determining significant prostate cancer is tumor volume. Although differences exist in whether tumor volume is an independent prognostic factor, it can be an important variable to consider in conjunction with other factors. Cancer volume has been shown to strongly correlate with the percentage of poorly differentiated cancer and nodal metastases (18). Currently, a cut-off figure of 0.5 cc is commonly used to distinguish insignificant from clinically significant cancer (19). Stamey *et al.* evaluated 139 cystoprostatectomy specimens where the procedure was undertaken within bladder cancer management (20). From the specimens the largest 8% of prostate cancers identified ranged in volume from 0.5–6.1 mL and within these only 20% patients had clinically significant prostate cancer. Other studies have placed this at 1.3 cc for pure Gleason 6 cancers. Bostwick *et al.* reviewed 9 studies, and concluded that tumor volume was a good positive predictor for several measures of tumor progression (21). Tumors measuring 0.5 cc had a 10% risk of capsular invasion, those measuring 4 cc had 10% risk of seminal vesicle invasion, and tumors measuring 5 cc had a 10% risk of metastases.
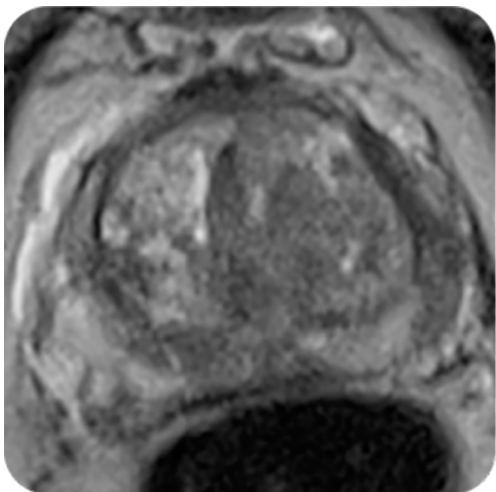
MRI of the prostate

MRI offers a more accurate modality than TRUS for both detection and localization of prostate cancer (22). Furthermore, the high resolution and soft tissue contrast allows for accurate local staging.

T1W imaging

T1W images have a limited role in evaluation of prostate cancer. T1W MRI images are sub-optimal for cancer detection as tumors show up as iso-intense to the prostate
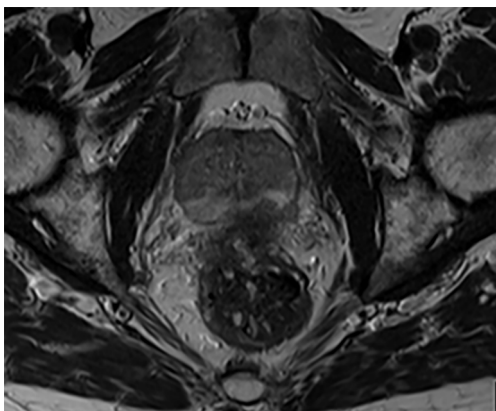
Figure 1 Capsular irregularity with no clear plane between prostate gland and adjacent anterior rectum at left posterior aspect of gland. T2 imaging.

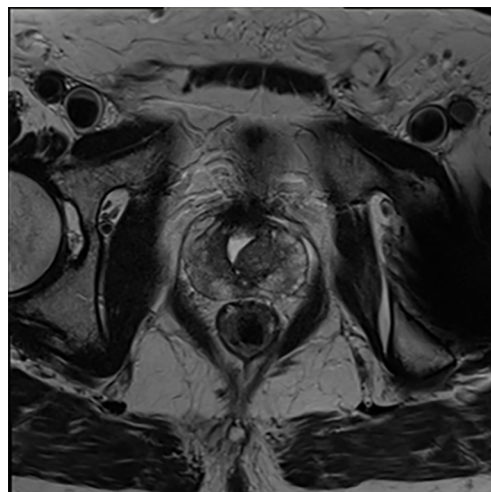**Figure 3** Area of high intensity secondary to a TURP defect.

Figure 2 Crescent of low T2 signal in anterior horn of left mid and basal gland, likely tumour.

gland. Areas of high water content emit low signal allowing for poor differentiation between metastatic and normal tissue (23). Hemorrhage will demonstrate hyperintensity on T1W images thus comparison may be made with T2-MRI when evaluating for post-biopsy hemorrhage (24,25).

T2W imaging

T2W imaging provides useful delineation of the zonal anatomy of the prostate gland, although it lacks the diagnostic accuracy to be used in isolation. The peripheral zone (PZ) of the prostate appears as an area of high signal intensity whereas the central gland has variable signal intensity. Prostate cancer in the PZ can appear as an area of hypo-intense signal compared to the higher signal depicting normal prostatic tissue (*Figures 1,2*).

This is secondary to the reduced free-water content of highly dense tumors and studies have demonstrated a positive correlation between the reduction in signal intensity and higher Gleason score parameters (26). The central zone may be replaced by well-circumscribed nodules related to benign prostatic hyperplasia (BPH) or interventions undertaken for its management (*Figure 3*).

However, T2W imaging alone can be inaccurate, as some tumors can be isointense. Furthermore, a low signal intensity on T2W is also seen in benign situations such as prostatitis, BPH, scarring and post-biopsy hemorrhage, which can mimic cancer. For this reason, when utilized in staging it is recommended that biopsy and T2 MRI be conducted with a minimum interval of 6-week (27). T2W MRI lacks the diagnostic accuracy to be used in isolation.

DWI

DWI assesses the ease with which water molecules move around within prostatic interstitial space. Rate of water diffusion in prostatic tissue is dependent on stromal density and tissue interstitial water, thus DWI reflects changes that may be caused by neoplastic growths within the organ. Prostate cancer results in increased cellularity, and a reduction of the extracellular space, and results in restricted diffusion on DWI.

S424

Lovegrove et al. Parameters on MRI that may warrant deferring prostate biopsy
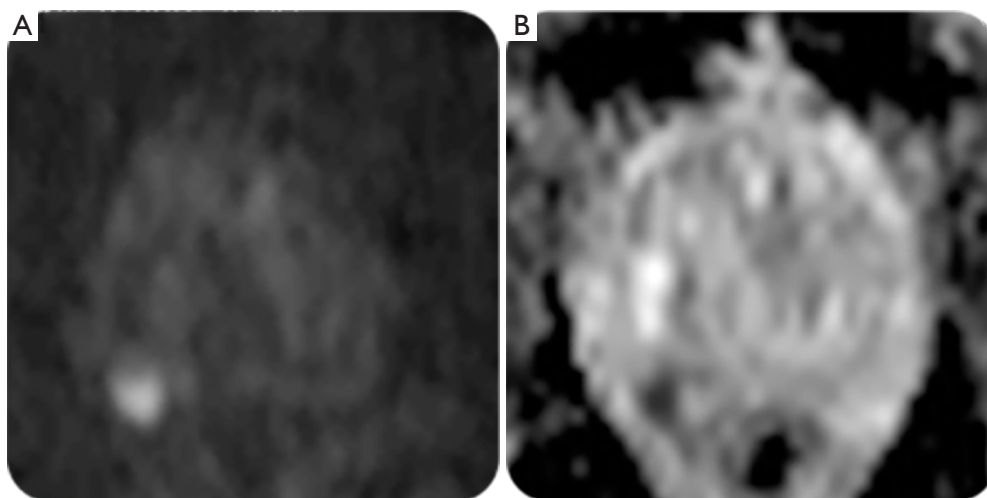
Figure 4 Utilizing diffusion weighted-imaging. (A) long b axial image, hyperintense tumour lesion right posterolateral zone, (B) hypointense lesion on ADC image.
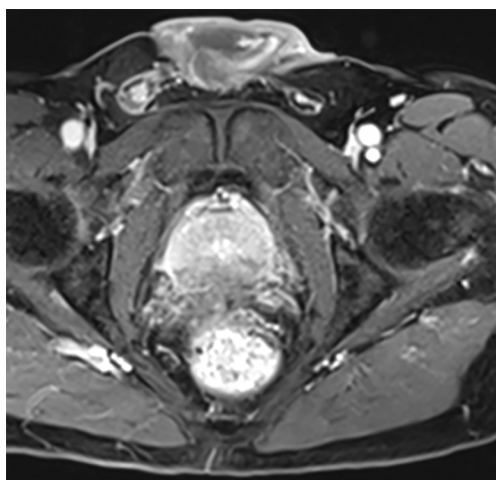
Figure 5 Reduced enhancement of left posterior peripheral zone on DCE, concerning for T4 disease.

The strength and duration of the diffusion gradient detected are referred to as "b-values" with higher values resulting in the production of a higher signal intensity (*Figure 4A*). Calculation of aforementioned b-values facilitates the construction of an apparent diffusion coefficient (ADC) map that demonstrates tumors as having low signal intensity secondary to the increased cell density, reduced interstitial fluid and reduced free water when compared to normal prostatic tissue such as that in a normal gland or in BPH (*Figure 4B*).

DWI has shown greater sensitivity, specificity and negative predictive value compared to PSA measurements and T2W imaging and has a more positive correlation with Gleason score and tumor volume (28,29). However, there exists an overlap between ADC values obtained in malignant and benign tissue especially nearing central and transitional zones of the prostate.

DCE imaging

DCE imaging utilizes intravenous gadolinium contrast to demonstrate the microvascular properties, angiogenesis and resulting perfusion rate in tissues. Serial imaging of wash-in and wash-out periods enables tumors to be identified and correlates with tumor aggression (30). Malignant prostate lesions have increased tumor vascularity, and show early, rapid and intense enhancement, followed by quick washout of contrast administered for imaging purposes (*Figure 5*).

Prostate cancer, chronic prostatitis and normal prostatic tissue demonstrate different vascular properties facilitating differentiation via DCE imaging. Vascular changes demonstrated by DCE MRI are also more distinct in high-grade disease and sequences can be particularly useful for cancers which are not apparent on T2W imaging. DCE has shown high sensitivity and specificity in delineating malignant versus benign prostatic tissue with improved tumor localization compared with T2 weighted imaging (31,32). However, there can be difficulties in distinguishing prostatitis from malignancy in the PZ, and between BPH and malignancies in the transition zone (TZ) with this

Table 2 PI-RADS v2 assessment categories

Score	Description of scores
PIRADS 1	Very low (clinically significant cancer is highly unlikely to be present)
PIRADS 2	Low (clinically significant cancer is unlikely to be present)
PIRADS 3	Intermediate (the presence of clinically significant cancer is equivocal)
PIRADS 4	High (clinically significant cancer is likely to be present)
PIRADS 5	Very high (clinically significant cancer is highly likely to be present)

modality.

Scoring systems for prostate MRI

Although MRI has been shown to be a powerful tool in the assessment and diagnosis of prostate cancer, one of the significant drawbacks is inter-rater variability. Standardization of prostate MRI reporting has been attempted using various scoring systems.

PI-RADS

To facilitate standardization in the reporting of prostate MRI, the European Society of Urogenital Radiology (ESUR) developed the Prostate Imaging and Report and Data System (PI-RADS v1) scoring system, published in 2012 (33). This formalized MRI reporting though lacked guidance on production of an overall score thus resulting in heterogeneity in reporting. It was subsequently updated to PI-RADS v2 in 2014 by the PI-RADS Steering Committee. PI-RADS v2 is designed to improve the detection, localization, characterization and risk stratification in patients with suspected cancer in treatment naive prostate glands (27,34).

PI-RADS v2 assessment uses a 5-point scale based on the likelihood that a combination of MP-MRI findings on T2W, DWI, and DCE correlates with the presence of a clinically significant cancer for each lesion in the prostate gland (*Table 2*).

Compared to PI-RADS v1, the updated scoring system introduced the principle of a dominant sequence, according to which zone of the prostate was being assessed. For the peripheral zone, DWI is considered the dominant sequence, and T2WI for the TZ. DCE is employed in PZ imaging when DWI results are equivocal. Further inter-reader standardization is ensured with an algorithm based on the individual sequence and zone scores, allowing an overall

score from 1 to 5 to be given in the final report. Head to head comparisons of PI-RADS v1 and PI-RADS v2 have shown mixed results. Overall, PI-RADS v2 appears to have greater diagnostic accuracy for TZ lesions, whereas PZ lesions are better evaluated with PI-RADS v1 (35).

Likert scale

The Likert scale is a visual analogue scale, where scores of 1–5 represent the likelihood of cancer based on the radiologist's overall interpretation of a prostate MRI scan (36). It does not require individual scoring assessment of separate sequences but an overall impression made by the radiologist. Scores of 1 and 2 represent a low suspicion of cancer, a score of 3 is equivocal, and a score of 4 or 5 is considered a high suspicion. Some studies have shown a good correlation with Likert scoring in detecting clinically significant cancers (37). Compared to PI-RADS v1, there appears to be good inter-reader reproducibility in the PZ. However, in the TZ, the Likert scale performed better (38). The Likert scale scoring system does lack reproducibility outside of expert radiologist hands, requiring training to improve diagnostic accuracy (38).

Evidence for MP-MRI as a triage test

The ability of MP-MRI to rule-out clinically significant disease and allow men to safely avoid a biopsy is measured using the negative predictive value (NPV). Early retrospective studies found a wide variation in diagnostic accuracy with NPV ranging from 58–95% (39). This has been addressed in the recent PROstate MR Imaging Study (PROMIS) which assessed the ability of MP-MRI to identify men who can safely avoid unnecessary biopsy (40). MP-MRI was shown to have excellent performance characteristics with a sensitivity of 93% (95% CI, 88–96%) and NPV of 89% (95% CI, 93–94%). If introduced as a

S426

Lovegrove et al. Parameters on MRI that may warrant deferring prostate biopsy
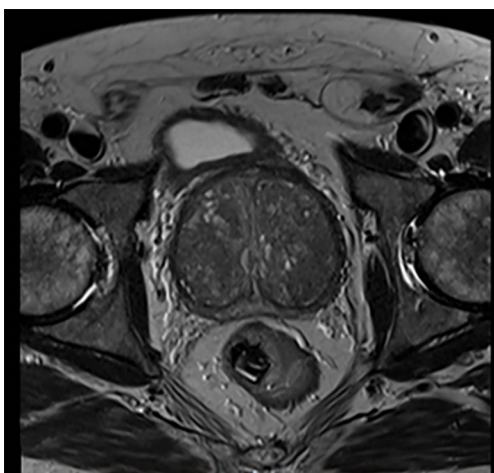
Figure 6 BPH with stromal nodules.

Figure 7 Nodular hyperplasia of TZ with low probability of significant tumour.

triage test it was estimated that it would lead to a 27% reduction in men requiring a prostate biopsy. The study was multi-center and these performance characteristics were reproducible across a range of centers and radiologists. All MRIs were performed on 1.5 Tesla scanners without an endorectal coil, which was chosen due to it wide availability across all centers.
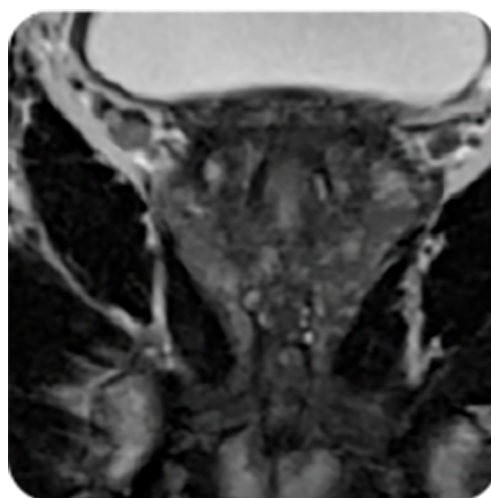
When considering whether MP-MRI can be used as a triage test, it is useful to compare to TRUS biopsy which has been the gold standard test over the last two decades. In PROMIS, TRUS biopsy was confirmed to be an inaccurate test with a sensitivity of 48% and NPV of 74% (95% CI, 69–78) (40). The risk of missing disease is significantly higher with a TRUS biopsy as it is blind to the location of the cancer. In addition, TRUS-biopsy is associated with significant morbidity and over diagnosis of clinically insignificant disease due the random nature of the biopsy technique.

Benign features on MRI

BPH

BPH nodules are seen as encapsulated round nodules with circumscribed margins. If they are predominantly glandular, they show T2 hyperintensity, whereas stromal nodules show T2 hypointensity. On DWI they can show a range of signal intensities, and may be highly vascular on DCE.

BPH typically occurs in the TZ with formation of large, discrete, encapsulated nodules formed by the hyperplasia of stromal and epithelial cells (*Figure 6*).

On T2-weighted imaging BPH results in a heterogeneous appearance which may be hypo-intense, iso-intense or hyper-intense according to the ratio of glandular to stromal tissue (41). Appreciation of the different BPH subtypes is critical in identification of malignant lesions (42). Glandular, cystic tissue responsible for prostatic secretions shows as high signal intensity on T2 weighted images and can be differentiated from neoplastic lesions owing to the different tissue properties. Conversely, mixed or sclerotic BPH nodules are composed of sclerotic, fibrous or muscular tissue resulting in hypo-intense lesions that can mimic neoplastic lesions within the TZ (*Figure 7*).

Stromal nodules also result in reduced signal intensity on DWI and early enhancement on DCE imaging, similar to cancerous tissue (43) (*Figure 8*).

In some cases, BPH may be found in PZ tissue and resemble prostate cancer. Well-defined, rounded lesions with internal heterogeneity on T2 weighted MRI are suggestive of benign hyperplasia over cancer.

Hemorrhage

Prostatic hemorrhage, commonly seen after biopsy, usually presents in the PZ. Cancerous tissue has a lower rate of hemorrhage than normal prostatic tissue as it has reduced levels of citrate, acting as an anti-coagulant and promoting resolution of hemorrhage faster than in the normal tissue (44). It is therefore possible that areas of prostate devoid of hemorrhage post-biopsy may be sites with positive biopsy
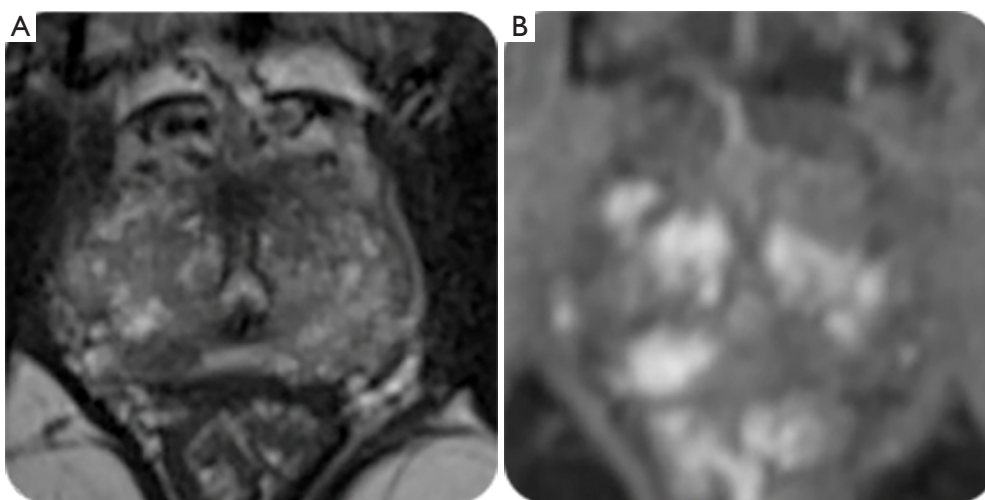
Figure 8 Similarities between stromal nodules and tumour tissue. (A) T2 hypointensity at right apex; (B) hyperintensity of same lesion on DCE, likely tumour.
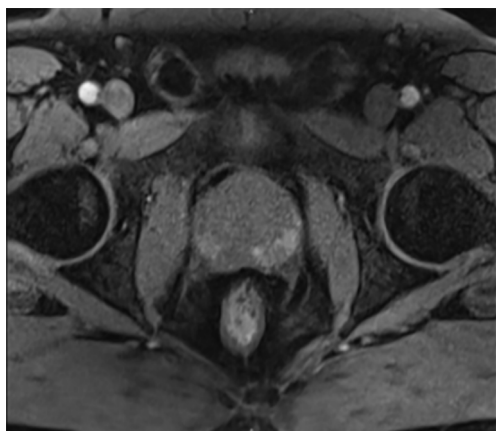
Figure 9 Post-biopsy prostatic haemorrhage.

findings (*Figure 9*).

The relationship between time and post-biopsy prostatic hemorrhage has led to the recommendation of an interval of at least six weeks and ideally 3 months between biopsy and imaging (27).

Bleeding results in variably low signal intensity on T2 weighted MRI depending on the time since biopsy whereas hemorrhage will be hyper-intense on T1 imaging. The high signal found on T1 MRI can limit the interpretation and yield of DCE studies with reduced differentiation between the high signal from areas of hemorrhage and enhancing malignant tissue. The variability in time since biopsy and signal intensity on MRI is also demonstrated

on DWI although prostate cancer will result in a lower ADC compared to hemorrhage. Comparison of areas of hyper-intensity on T2 and DWI MRI with T1 weighted images allows application of the "hemorrhage exclusion sign", facilitating delineation between lesions that are hemorrhagic in nature or cancerous in nature (44). Presence of the hemorrhage exclusion sign on T1 images (reduced signal intensity) and corresponding hypo-intensity on T2W imaging has shown a positive predictive value of approximately 95% for prostate cancer lesions (23).
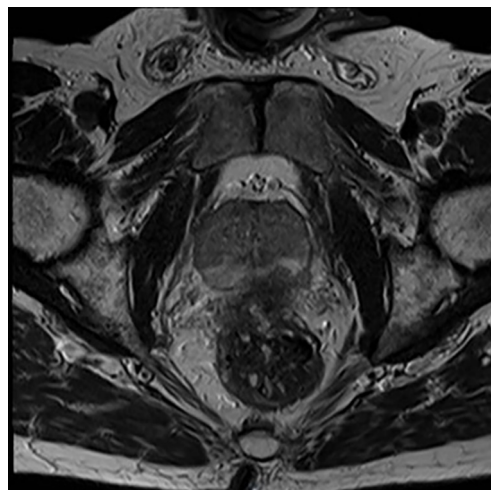
Cysts

Simple prostatic cysts will usually appear hyper-intense on T2W and hypo-intense on T1W, but may also show T1W hyper-intensity if they contain blood products or proteinaceous fluids (45) (*Figure 10*).

Following pelvic lymphadenectomy, lymphoceles may form along lymph node chains in the pelvic and para-aortic regions. Like simple prostatic cysts, these too demonstrated hypo-intensity on T1 weighted images and high-intensity on T2 images. Following administration of gadolinium contrast IV they do not enhance. Anatomical location is also useful in delineating such lesions from prostate cancer as they are located along lymph node chains dissected at the time of surgery whereas structural defects are identified nearby the tissue of origin, as with urethral diverticula (*Figure 11*).
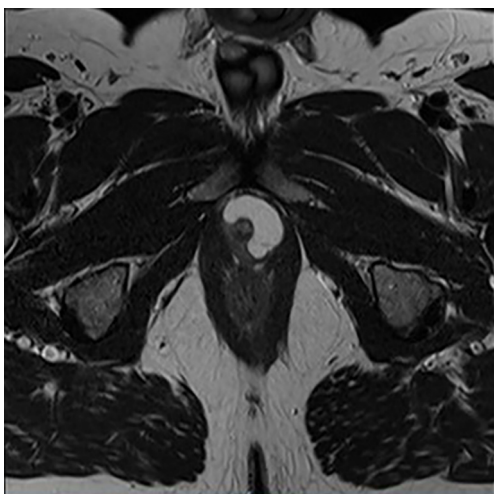
tau.amegroups.com   *Transl Androl Urol* 2018;7(Suppl 4):S420-S435
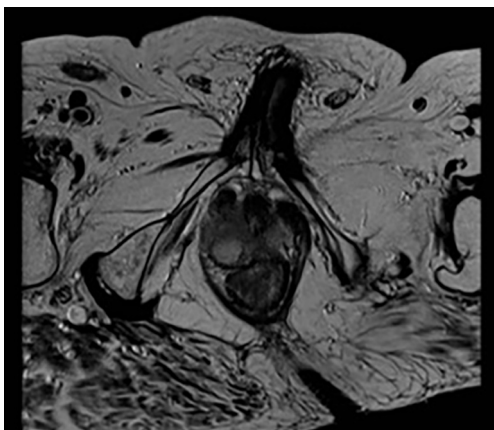
Figure 10 17 mm cystic lesion at right peripheral zone apex.

Figure 11 Crescent-shaped urethral diverticulum surrounding membranous urethra.

Prostatitis

Prostatitis results in the formation of an immune infiltrate, the character of which depends on the cause of the inflammation (45). It demonstrates a diffuse, band-like, wedge-shaped morphology that may distinguish it from prostate cancer lesions which are more commonly round, oval or irregular and have a more focal decrease in signal attenuation on ADC mapping (*Figure 12*).

However, extensive granulomatous prostatitis, for example secondary to BCG administration in bladder cancer therapy, may result in extra-capsular extension of the inflammation which can be more difficult to distinguish form malignant lesions (46,47).

Figure 12 Prostatitis identified on MRI.

With regards to imaging modalities, granulomatous prostatitis can manifest similarly to cancer with low signal intensity on T2 MRI, irregular margins and variable morphology found in the PZ (48). Reduction in T2 signal intensity may be secondary to calcification, fibrosis, or non-caseating necrosis. ADC is also reduced secondary to high cellular density. Areas of inflammation may increase perfusion on DCE sequences giving rise to a false-positive finding. However, DCE enhancement secondary to prostatitis is usually not as marked as found in prostate cancer.

Converse to non-specific granulomatous prostatitis, necrotizing granulomatous prostatitis results in necrosis with increased signal intensity on T2 imaging, marked hyper-intensity on ADC mapping secondary to increased diffusion restriction and non-enhancing lesions on DCE MRI.

Atrophy

Prostatic atrophy results from inflammation, chronic ischemia and exposure to radiation or anti-androgens. Microscopically, prostatic atrophy demonstrates crowded glands, scant cytoplasm and crowded nuclei when compared to prostatic tissue. There exist several sub-types including simple, sclerotic with cysts and post-atrophic hyperplasia. The glandular crowding present in the latter with complex glandular architecture can frequently be mistaken as malignant. In addition, there exists a positive correlation between the extent of prostatic atrophy and PSA elevation

Figure 13 Prostatic atrophy in peripheral zone on T2-MRI.

Figure 14 T2 image with medial-mid right peripheral zone wedge-shaped hypodensity suggestive of fibrosis. Incidental midline Mullerian duct remnant.

likely released from damaged prostatic tissue (49).

On imaging, focal atrophy is more commonly located in the PZ with low signal intensity on T2 weighted imaging, moderate enhancement on DCE MRI and moderate restriction of diffusion in DWI (*Figure 13*).

The lower rate of diffusion and reduced signal intensity is not as evident as that of cancerous lesions and is usually accompanied by loss of tissue volume. DWI and DCE images have been reported to result in a higher diagnostic yield in cases of prostatic atrophy and T2 MRI, more so than for other benign prostatic lesions (50).

Fibrosis

Fibrosis following inflammation or post-operative fibrosis results in wedge-shaped or band-shaped areas of hypo-intensity on all MRI sequence modalities (45,51) (*Figure 14*).

Quantitative MRI

Advances in MRI techniques have facilitated increased sensitivity of prostate cancer detection and prediction of Gleason score. However, interpretation can be limited by the vast amounts of data amassed for each patient from each sequencing modality. Standardization is crucial in reducing inter-rater reliability and the accuracy of diagnosis of benign or malignant lesions. Computer aided diagnosis (CAD) utilizes software to aid radiologists in detecting and diagnosing abnormalities from diagnostic imaging. One such example is the quantitative analysis of diffusion

properties within prostatic tissue through measurement of the ADC in DWI MRI (52). As demonstrated above, this imaging technology is currently limited by reliance on the underlying tissue microstructure and is not specific to histological features found in cancerous masses compared to benign tissue.

New techniques of quantitative MRI use tissue-specific factors to delineate different cellular and microstructural phenotypes. VERDICT MRI (vascular, extracellular and restricted diffusion for cytometry in tumors) is a technique that maps the histological features of tissues by combining DWI with a mathematical model to provide information on cell size, density, extracellular-extravascular space volume fraction and vascularity via pseudo-diffusion coefficient associated with blood flow. It utilizes three main components to produce this information; vascular, extracellular-extravascular space and intracellular water. These factors influence the DWI signal produced and by application to different diffusion times and weightings provides a more effective delineation of tissue microstructure than ADC from DWI MRI. In contrast to conventional histology of tissue samples, VERDICT MRI can characterize the micro-structure of a whole tumor enabling more reliable information surrounding its properties and likelihood of possessing cancerous properties.

Panagiotaki *et al.* demonstrated its effectiveness through analysis of colorectal carcinoma xenografts where VERDICT MRI was able to characterize tumor type,

distinguish the microstructure of tumor histology and confirm tissue response to gemcitabine chemotherapy (53). On application to prostate cancer the technique was able to demonstrate increased intracellular and vascular volume fraction in cancerous compared to benign peripheral zone tissue which correlated with findings from histological specimens (P=0.05) (54). ADC and Kurtosis parameters were also able to distinguish benign from cancerous tissues though with less specific information than VERDICT.

MP-MRI and tumor volume

A MP-MRI derived tumor volume can be calculated using via manual measurements or 3-dimensional analysis software. The volume of the index lesion is a well-established histological prognostic factor and traditionally set at 0.5 cc as described in the previous section of this article. The level of accuracy of MP-MRI volumetry remains under debate although the majority of studies have concluded that MP-MRI provides a reasonable estimation compared to volume on whole mount histology (55). The accuracy is greater for tumors over 10mm in diameter and larger than 0.5 cc in volume (56). MP-MRI does tend to systematically underestimate tumor volume and multiple studies have shown that the tumor extends beyond the boundaries of the visible portion of tumor on MRI (57). For this reason, when using MP-MRI to guide focal therapy rather than aiming to ablate the visible MRI tumor an additional safety margin should be defined (58).

Functional imaging

There are a number of functional imaging methods which determine the metabolic activity of prostatic tissue (59). Molecular imaging refers to measuring biological processes to visualize and characterize tissues at both molecular and cellular levels. These techniques tend to have lower spatial resolution and the ability to image physiological processes provides valuable diagnostic information.

MR spectroscopy

Proton MR spectroscopic imaging (MRSI) is a more technically challenging imaging modality than DCE and DWI MRI especially in the processing of images to create an acceptable output. This can be attributed to metabolites (citrate, creatinine, polyamines, and choline-containing compounds) being of low signal intensity and

the surrounding tissues being relatively lipid-rich (60). As previously mentioned, the presence of citrate in malignant tissue can aid differentiation from benign masses and MRSI utilizes the ratio of choline plus creatinine to citrate (CC/C) as a marker of cancer tissue. Studies have demonstrated the effectiveness of this as a marker of identifying cancer versus non-cancer in both the peripheral and central gland (61). Differences between median values of CC/C were observed between centers participating in the study. This finding may be attributed to heterogeneity in histopathologic information or size of cancer foci. Fusco *et al.* found significant differences between clinically significant and insignificant prostate cancer on MR spectroscopy thus increasing the sensitivity and specificity in correlating with prostate biopsy results (62). Furthermore their study demonstrated disparities using different molecular markers but that optimum outcomes were achieved when combining the parameters of perfusion, diffusion and metabolism. However, other studies have failed to replicate such findings and have found that benign disease, such as chronic prostatitis, produced images that were indistinguishable from prostate cancer (63). Careful selection of metabolites and their ratios for analysis can facilitate comparison between different fields and acquisition schemes or automation of post-processing has potential to increase the reliability of ratio maps obtained to facilitate clinical utility (60).

Choline and prostate-specific membrane antigen (PSMA) positron emission tomography (PET)

An emerging image modality is PET with prostate cancer-specific tracers. Over the last decade, this technique has developed as a better diagnostic tool for staging than conventional imaging. The conventional staging techniques involve bone scan for metastatic disease and nodal staging using CT or MRI which relies on changes to the morphology or size of lymph nodes. A meta-analysis of CT and MRI shows that these conventional techniques have a poor sensitivity of 39–42% and specificity of 82% for accurate lymph node staging (64).

In other tumor groups, the most common PET/CT tracer is ^{18}F-FDG as a measurement of glycolytic activity of cells but in the context of prostate cancer it has not been effective (65). Localized prostate cancer tends to have low metabolic glycolytic activity compared to other cancers. FDG is also taken up by BPH nodules and the renal excretion of FDG means the high concentration in

the bladder can mask prostate tumors. Instead, choline-based tracers have been introduced which detect the higher rate of lipid metabolism in prostate cancer cells. However due to their limited sensitivity, the current guidelines do not recommend using them for lymph node staging (66). Evangelista *et al.* completed a meta-analysis on the diagnostic accuracy of choline-based tracers showing a sensitivity of 39.2% and specificity of 95% for lymph node detection (67).

Following the limitations of choline and FDG-tracers, there is a need for tracers with improved accuracy. PSMA is showing significant potential. PSMA is a transmembrane protein with a 707-amino-acid extra cellular portion which is expressed in the apical region and epithelium around prostatic ducts (68). Despite being expressed in healthy prostate tissue, it's overexpression on the cell membrane of prostate cancer cells makes it a promising target for functional imaging (69). PSMA is involved in the cellular uptake of folate which makes it a growth factor to malignant cells. Therefore, there are high levels of PSMA expression in metabolically active cells. As such, it is a marker of disease activity and is increased for higher Gleason scores (70). There is a growing body of evidence supporting the use of PSMA in primary staging. A meta-analysis including 1,309 patients reported a sensitivity and specificity of 86% across sixteen articles involving 1,309 patients.

Hyperpolarized MRI

Hyperpolarization refers to the *ex vivo* application of increased spin polarization to small molecules and then administration with MRI to allow the visualization of the molecule's metabolism *in vivo*. The increased polarization increases the signal produced by up to 10,000 times compared to that which is produced by physiological concentrations of the molecule on standard MRI (71). ^{13}C-pyruvate has been employed for this technology, via microwave irradiation through transfer of hyperpolarized electrons.

Nelson *et al.* first demonstrated the feasibility and safety of hyperpolarized MRI in men with prostate cancer on active surveillance (72). They demonstrated increased signal intensity in areas of the prostate that included tumor and low or undetectable signal from normal prostatic tissue which converts four to five times less pyruvate to lactate than malignant tissue. The technique was able to delineate regions of biopsy-proven tumor that had not been located during staging examination by MP-MRI, demonstrating the potential for hyperpolarized MRI to increase diagnostic yield and differentiate high-grade, low-grade and benign tissue. Additionally, the same group was

able to illustrate the technique's effectiveness as a biomarker of response to androgen deprivation therapy where T2 weighted imaging and ADC had limited change between pre-treatment and post-treatment imaging. This response correlated with clinical response to therapy where the patient reached a PSA nadir after six months (73).

While hyperpolarized MRI shows promise in improving the imaging and differentiation of benign and malignant lesions, there is work to be done before recommending more widespread use (74). For example, for its application there is a need to identify suitable molecules for hyperpolarization through analysis of metabolic pathways within tumor tissue and cancer-specific biomarkers. Technology for storage of hyperpolarized molecules and protocols for quality assurance, reproducibility and reduction of inter-rater variability needs investment and larger, more wide-spread studies are necessary.

Discussion

Discrimination between benign and malignant lesions on imaging is an important element in identification of patients who require invasive investigations and potentially treatment for prostate cancer. Current reliance on TRUS-guided biopsy subjects patients to an uncomfortable procedure which has associated risks and has been linked with the over-diagnosis and over-treatment of low-grade disease and oversight of more concerning, aggressive disease (75). Several MRI techniques have evolved that can aid radiologists, clinicians and surgeons in evaluating prostatic lesions, notably quantitative MRI and functional imaging. However benign condition such as BPH, hemorrhage, cysts, prostatitis, atrophy, and fibrosis can occasionally mimic cancer and more novel techniques show promise in furthering the ability to discern between benign and malignant disease.

Thus, appearance of abnormalities on MRI is not the only parameter to be borne in mind particularly when trying to distinguish which patients need a biopsy. Muthigi *et al.* found a lower PSA, higher prostate volume, and fewer targeted cores were seen to be predictors of upgrading on systematic biopsy when compared to those patients who underwent biopsies targeted only at a MRI lesion (76).

There is evidence to suggest that the negative predictive value in patients with a negative MRI and a PSA density of ≤0.2 ng/mL is 0.91 for the detection of Gleason score ≥7 prostate cancer and thus these patients could safely avoid biopsy (77). Conversely, those with a PSA density of ≥0.2 and a negative or equivocal MRI should undergo biopsy as

tau.amegroups.com

S432

Lovegrove et al. Parameters on MRI that may warrant deferring prostate biopsy

they may harbor clinically significant disease (NPV 0.71) (78,79). Others such as Venderink *et al.* have reported on a PSA density threshold of 0.15 ng/mL as the cut-off for biopsy in patients with a PIRADS 3 lesion. They found that utilizing this threshold would have avoided biopsy in 42% of patients with a PIRADS 3 lesion, whilst only 6% of clinically significant cancer would have been missed (80).

Similarly promising results were obtained by Rayn *et al.* when examining findings from MP-MRI with existing staging nomograms that incorporate PSA, Gleason Grade Group and clinical staging. The study found that smaller lesion diameter on MP-MRI was the strongest predictor for organ-confined disease and for non-organ confined disease the MP-MRI findings had greater predictive value than Partin and Memorial Sloan Kettering Cancer Centre nomograms alone. Addition of MP-MRI to staging nomograms significantly improves prediction of organ-confined disease, extraprostatic extension and seminal vesicle invasion increasing the predictive ability of adverse features at the time of radical prostatectomy.

Emergence of biomarkers may also change the diagnostic landscape allowing stratification of patients alongside a MRI with tests such as PHI showing promise, however significant research in this his field is needed prior to their widespread utilization (81).

Acknowledgements

Footnote

Conflicts of Interest: HU Ahmed proctors for HIFU and cryotherapy and is paid for training other surgeons in these procedures. HU Ahmed is a paid medical consultant for Sophiris Biocorp and Sonacare Inc. M Winkler receives a travel grant and a loan of device from Zicom Biobot. Other authors have no conflicts of interest to declare.

References

1. Dickinson L, Ahmed HU, Allen C, et al. Magnetic resonance imaging for the detection, localisation, and characterisation of prostate cancer: recommendations from a European consensus meeting. Eur Urol 2011;59:477-94.

2. Seo JW, Shin SJ, Taik Oh Y, et al. PI-RADS Version 2: Detection of Clinically Significant Cancer in Patients With Biopsy Gleason Score 6 Prostate Cancer. AJR Am J Roentgenol 2017;209:W1-9.

3. Ploussard G, Epstein JI, Montironi R, et al. The contemporary concept of significant versus insignificant prostate cancer. Eur Urol 2011;60:291-303.

4. Hanahan D, Weinberg RA. Hallmarks of cancer: the next generation. Cell 2011;144:646-74.

5. Ahmed HU, Arya M, Freeman A, et al. Do low-grade and low-volume prostate cancers bear the hallmarks of malignancy? Lancet Oncol 2012;13:e509-17.

6. Gleason DF, Mellinger GT. Prediction of prognosis for prostatic adenocarcinoma by combined histological grading and clinical staging. J Urol 1974;111:58-64.

7. Epstein JI, Allsbrook WC Jr, Amin MB, et al. The 2005 International Society of Urological Pathology (ISUP) Consensus Conference on Gleason Grading of Prostatic Carcinoma. Am J Surg Pathol 2005;29:1228-42.

8. Latour M, Amin MB, Billis A, et al. Grading of invasive cribriform carcinoma on prostate needle biopsy: an interobserver study among experts in genitourinary pathology. Am J Surg Pathol 2008;32:1532-9.

9. Danneman D, Drevin L, Robinson D, et al. Gleason inflation 1998-2011: a registry study of 97,168 men. BJU Int 2015;115:248-55.

10. Pierorazio PM, Walsh PC, Partin AW, et al. Prognostic Gleason grade grouping: data based on the modified Gleason scoring system. BJU Int 2013;111:753-60.

11. Helpap B, Egevad L. The significance of modified Gleason grading of prostatic carcinoma in biopsy and radical prostatectomy specimens. Virchows Arch 2006;449:622-7.

12. Billis A, Quintal MM, Meirelles L, et al. The value of the 2005 International Society of Urological Pathology (ISUP) modified Gleason grading system as a predictor of biochemical recurrence after radical prostatectomy. Int Urol Nephrol 2014;46:935-40.

13. Pan CC, Potter SR, Partin AW, et al. The prognostic significance of tertiary Gleason patterns of higher grade in radical prostatectomy specimens: a proposal to modify the Gleason grading system. Am J Surg Pathol 2000;24:563-9.

14. D'Amico AV, Whittington R, Malkowicz SB, et al. Biochemical outcome after radical prostatectomy,

external beam radiation therapy, or interstitial radiation therapy for clinically localized prostate cancer. JAMA 1998;280:969-74.

15. Epstein JI, Zelefsky MJ, Sjoberg DD, et al. A Contemporary Prostate Cancer Grading System: A Validated Alternative to the Gleason Score. Eur Urol 2016;69:428-35.

16. Wheeler TM, Dillioglugil O, Kattan MW, et al. Clinical and pathological significance of the level and extent of capsular invasion in clinical stage T1-2 prostate cancer. Hum Pathol 1998;29:856-62.

17. Hull GW, Rabbani F, Abbas F, et al. Cancer control with radical prostatectomy alone in 1,000 consecutive patients. J Urol 2002;167:528-34.

18. McNeal JE, Villers AA, Redwine EA, et al. Histologic differentiation, cancer volume, and pelvic lymph node metastasis in adenocarcinoma of the prostate. Cancer 1990;66:1225-33.

19. Stamey TA, Yemoto CE. Examination of the 3 molecular forms of serum prostate specific antigen for distinguishing negative from positive biopsy: relationship to transition zone volume. J Urol 2000;163:119-26.

20. Stamey TA, Freiha FS, McNeal JE, et al. Localized prostate cancer. Relationship of tumor volume to clinical significance for treatment of prostate cancer. Cancer 1993;71:933-8.

21. Bostwick DG, Graham SD Jr, Napalkov P, et al. Staging of early prostate cancer: a proposed tumor volume-based prognostic index. Urology 1993;41:403-11.

22. Bonekamp D, Jacobs MA, El-Khouli R, et al. Advancements in MR imaging of the prostate: from diagnosis to interventions. Radiographics 2011;31:677-703.

23. Barrett T, Vargas HA, Akin O, et al. Value of the hemorrhage exclusion sign on T1-weighted prostate MR images for the detection of prostate cancer. Radiology 2012;263:751-7.

24. Villers A, Lemaitre L, Haffner J, et al. Current status of MRI for the diagnosis, staging and prognosis of prostate cancer: implications for focal therapy and active surveillance. Curr Opin Urol 2009;19:274-82.

25. Shah TT, To WKL, Ahmed HU. Magnetic resonance imaging in the early detection of prostate cancer and review of the literature on magnetic resonance imaging-stratified clinical pathways. Expert Rev Anticancer Ther 2017;17:1159-68.

26. Wang L, Mazaheri Y, Zhang J, et al. Assessment of biologic aggressiveness of prostate cancer: correlation of MR signal intensity with Gleason grade after radical prostatectomy. Radiology 2008;246:168-76.

27. Weinreb JC, Barentsz JO, Choyke PL, et al. PI-RADS Prostate Imaging - Reporting and Data System: 2015, Version 2. Eur Urol 2016;69:16-40.

28. Hegde JV, Mulkern RV, Panych LP, et al. Multiparametric MRI of prostate cancer: an update on state-of-the-art techniques and their performance in detecting and localizing prostate cancer. J Magn Reson Imaging 2013;37:1035-54.

29. Tamada T, Sone T, Higashi H, et al. Prostate cancer detection in patients with total serum prostate-specific antigen levels of 4-10 ng/mL: diagnostic efficacy of diffusion-weighted imaging, dynamic contrast-enhanced MRI, and T2-weighted imaging. AJR Am J Roentgenol 2011;197:664-70.

30. Choyke PL, Dwyer AJ, Knopp MV. Functional tumor imaging with dynamic contrast-enhanced magnetic resonance imaging. J Magn Reson Imaging 2003;17:509-20.

31. Zelhof B, Lowry M, Rodrigues G, et al. Description of magnetic resonance imaging-derived enhancement variables in pathologically confirmed prostate cancer and normal peripheral zone regions. BJU Int 2009;104:621-7.

32. Futterer JJ, Heijmink SW, Scheenen TW, et al. Prostate cancer localization with dynamic contrast-enhanced MR imaging and proton MR spectroscopic imaging. Radiology 2006;241:449-58.

33. Barentsz JO, Richenberg J, Clements R, et al. ESUR prostate MR guidelines 2012. Eur Radiol 2012;22:746-57.

34. Barentsz JO, Weinreb JC, Verma S, et al. Synopsis of the PI-RADS v2 Guidelines for Multiparametric Prostate Magnetic Resonance Imaging and Recommendations for Use. Eur Urol 2016;69:41-9.

35. Polanec S, Helbich TH, Bickel H, et al. Head-to-head comparison of PI-RADS v2 and PI-RADS v1. Eur J Radiol 2016;85:1125-31.

36. Shin T, Smyth TB, Ukimura O, et al. Diagnostic accuracy of a five-point Likert scoring system for magnetic resonance imaging (MRI) evaluated according to results of MRI/ultrasonography image-fusion targeted biopsy of the prostate. BJU Int 2018;121:77-83.

37. Harada T, Abe T, Kato F, et al. Five-point Likert scaling on MRI predicts clinically significant prostate carcinoma. BMC Urol 2015;15:91.

38. Rosenkrantz AB, Lim RP, Haghighi M, et al. Comparison of interreader reproducibility of the prostate imaging reporting and data system and likert scales for evaluation of multiparametric prostate MRI. AJR Am J Roentgenol

2013;201:W612-8.

39. Hamoen EHJ, de Rooij M, Witjes JA, et al. Use of the Prostate Imaging Reporting and Data System (PI-RADS) for Prostate Cancer Detection with Multiparametric Magnetic Resonance Imaging: A Diagnostic Meta-analysis. Eur Urol 2015;67:1112-21.

40. Ahmed HU, El-Shater Bosaily A, Brown LC, et al. Diagnostic accuracy of multi-parametric MRI and TRUS biopsy in prostate cancer (PROMIS): a paired validating confirmatory study. Lancet 2017;389:815-22.

41. Kim CK, Park BK, Han JJ, et al. Diffusion-weighted imaging of the prostate at 3 T for differentiation of malignant and benign tissue in transition and peripheral zones: preliminary results. J Comput Assist Tomogr 2007;31:449-54.

42. Tamada T, Sone T, Jo Y, et al. Apparent diffusion coefficient values in peripheral and transition zones of the prostate: comparison between normal and malignant prostatic tissues and correlation with histologic grade. J Magn Reson Imaging 2008;28:720-6.

43. Kim CK, Park BK, Lee HM, et al. Value of diffusion-weighted imaging for the prediction of prostate cancer location at 3T using a phased-array coil: preliminary results. Invest Radiol 2007;42:842-7.

44. Purysko AS, Herts BR. Prostate MRI: the hemorrhage exclusion sign. J Urol 2012;188:1946-7.

45. American College of Radiology. PI-RADS. Prostate Imaging – Reporting and Data System Version 2. American College of Radiology. 2015. Available online: https://www.acr.org/-/media/ACR/Files/RADS/Pi-RADS/PIRADS-V2.pdf?la=en. Accessed 03.02.2018 2018.

46. Kitzing YX, Prando A, Varol C, et al. Benign Conditions That Mimic Prostate Carcinoma: MR Imaging Features with Histopathologic Correlation. Radiographics 2016;36:162-75.

47. Rais-Bahrami S, Nix JW, Turkbey B, et al. Clinical and multiparametric MRI signatures of granulomatous prostatitis. Abdom Radiol (NY) 2017;42:1956-62.

48. Bour L, Schull A, Delongchamps NB, et al. Multiparametric MRI features of granulomatous prostatitis and tubercular prostate abscess. Diagn Interv Imaging 2013;94:84-90.

49. Prando A, Billis A. Focal prostatic atrophy: mimicry of prostatic cancer on TRUS and 3D-MRSI studies. Abdom Imaging 2009;34:271-5.

50. Litjens GJS, Elliott R, Shih NN, et al. Computer-extracted Features Can Distinguish Noncancerous Confounding Disease from Prostatic Adenocarcinoma at Multiparametric

MR Imaging. Radiology 2016;278:135-45.

51. Panebianco V, Barchetti F, Barentsz J, et al. Pitfalls in Interpreting mp-MRI of the Prostate: A Pictorial Review with Pathologic Correlation. Insights Imaging 2015;6:611-30.

52. Peng Y, Jiang Y, Yang C, et al. Quantitative analysis of multiparametric prostate MR images: differentiation between prostate cancer and normal tissue and correlation with Gleason score--a computer-aided diagnosis development study. Radiology 2013;267:787-96.

53. Panagiotaki E, Walker-Samuel S, Siow B, et al. Noninvasive quantification of solid tumor microstructure using VERDICT MRI. Cancer Res 2014;74:1902-12.

54. Panagiotaki E, Chan RW, Dikaios N, et al. Microstructural characterization of normal and malignant human prostate tissue with vascular, extracellular, and restricted diffusion for cytometry in tumours magnetic resonance imaging. Invest Radiol 2015;50:218-27.

55. Bratan F, Melodelima C, Souchon R, et al. How accurate is multiparametric MR imaging in evaluation of prostate cancer volume? Radiology 2015;275:144-54.

56. Coakley FV, Kurhanewicz J, Lu Y, et al. Prostate cancer tumor volume: measurement with endorectal MR and MR spectroscopic imaging. Radiology 2002;223:91-7.

57. Langer DL, van der Kwast TH, Evans AJ, et al. Intermixed normal tissue within prostate cancer: effect on MR imaging measurements of apparent diffusion coefficient and T2--sparse versus dense cancers. Radiology 2008;249:900-8.

58. Le Nobin J, Rosenkrantz AB, Villers A, et al. Image Guided Focal Therapy for Magnetic Resonance Imaging Visible Prostate Cancer: Defining a 3-Dimensional Treatment Margin Based on Magnetic Resonance Imaging Histology Co-Registration Analysis. J Urol 2015;194:364-70.

59. Testa C, Pultrone C, Manners DN, et al. Metabolic Imaging in Prostate Cancer: Where We Are. Front Oncol 2016;6:225.

60. Scheenen TW, Rosenkrantz AB, Haider MA, et al. Multiparametric Magnetic Resonance Imaging in Prostate Cancer Management: Current Status and Future Perspectives. Invest Radiol 2015;50:594-600.

61. Scheenen TW, Futterer J, Weiland E, et al. Discriminating cancer from noncancer tissue in the prostate by 3-dimensional proton magnetic resonance spectroscopic imaging: a prospective multicenter validation study. Invest Radiol 2011;46:25-33.

62. Fusco R, Sansone M, Petrillo M, et al. Multiparametric MRI for prostate cancer detection: Preliminary results

on quantitative analysis of dynamic contrast enhanced imaging, diffusion-weighted imaging and spectroscopy imaging. Magn Reson Imaging 2016;34:839-45.

63. Shukla-Dave A, Hricak H, Eberhardt SC, et al. Chronic prostatitis: MR imaging and 1H MR spectroscopic imaging findings--initial observations. Radiology 2004;231:717-24.

64. Hovels AM, Heesakkers RA, Adang EM, et al. The diagnostic accuracy of CT and MRI in the staging of pelvic lymph nodes in patients with prostate cancer: a meta-analysis. Clin Radiol 2008;63:387-95.

65. Effert PJ, Bares R, Handt S, et al. Metabolic imaging of untreated prostate cancer by positron emission tomography with 18fluorine-labeled deoxyglucose. J Urol 1996;155:994-8.

66. European Association of Urology. Prostate Cancer. European Association of Urology. 2018. Available online: http://uroweb.org/guideline/prostate-cancer/. Accessed 05.02.2019 2018.

67. Evangelista L, Guttilla A, Zattoni F, et al. Utility of choline positron emission tomography/computed tomography for lymph node involvement identification in intermediate-to high-risk prostate cancer: a systematic literature review and meta-analysis. Eur Urol 2013;63:1040-8.

68. Afshar-Oromieh A, Avtzi E, Giesel FL, et al. The diagnostic value of PET/CT imaging with the (68)Ga-labelled PSMA ligand HBED-CC in the diagnosis of recurrent prostate cancer. Eur J Nucl Med Mol Imaging 2015;42:197-209.

69. Maurer T, Eiber M, Schwaiger M, et al. Current use of PSMA-PET in prostate cancer management. Nat Rev Urol 2016;13:226-35.

70. Silver DA, Pellicer I, Fair WR, et al. Prostate-specific membrane antigen expression in normal and malignant human tissues. Clin Cancer Res 1997;3:81-5.

71. Miloushev VZ, Keshari KR, Holodny AI. Hyperpolarization MRI: Preclinical Models and Potential Applications in Neuroradiology. Top Magn Reson Imaging 2016;25:31-7.

72. Nelson SJ, Kurhanewicz J, Vigneron DB, et al. Metabolic imaging of patients with prostate cancer using hyperpolarized [1-(1)(3)C]pyruvate. Sci Transl Med 2013;5:198ra108.

73. Aggarwal R, Vigneron DB, Kurhanewicz J. Hyperpolarized 1-[(13)C]-Pyruvate Magnetic Resonance Imaging Detects an Early Metabolic Response to Androgen Ablation Therapy in Prostate Cancer. Eur Urol 2017;72:1028-9.

74. Kurhanewicz J, Vigneron DB, Brindle K, et al. Analysis of cancer metabolism by imaging hyperpolarized nuclei: prospects for translation to clinical research. Neoplasia 2011;13:81-97.

75. Klotz L, Emberton M. Management of low risk prostate cancer: active surveillance and focal therapy. Curr Opin Urol 2014;24:270-9.

76. Muthigi A, George AK, Sidana A, et al. Missing the Mark: Prostate Cancer Upgrading by Systematic Biopsy over Magnetic Resonance Imaging/Transrectal Ultrasound Fusion Biopsy. J Urol 2017;197:327-34.

77. Filson CP, Natarajan S, Margolis DJ, et al. Prostate cancer detection with magnetic resonance-ultrasound fusion biopsy: The role of systematic and targeted biopsies. Cancer 2016;122:884-92.

78. Hansen NL, Barrett T, Koo B, et al. The influence of prostate-specific antigen density on positive and negative predictive values of multiparametric magnetic resonance imaging to detect Gleason score 7-10 prostate cancer in a repeat biopsy setting. BJU Int 2017;119:724-30.

79. Abdi H, Zargar H, Goldenberg SL, et al. Multiparametric magnetic resonance imaging-targeted biopsy for the detection of prostate cancer in patients with prior negative biopsy results. Urol Oncol 2015;33:165 e1-7.

80. Venderink W, van Luijtelaar A, Bomers JG, et al. Results of Targeted Biopsy in Men with Magnetic Resonance Imaging Lesions Classified Equivocal, Likely or Highly Likely to Be Clinically Significant Prostate Cancer. Eur Urol 2017. [Epub ahead of print].

81. Druskin SC, Tosoian JJ, Young A, et al. Combining Prostate Health Index density, magnetic resonance imaging and prior negative biopsy status to improve the detection of clinically significant prostate cancer. BJU Int 2018;121:619-26.